

An isotropic compact stellar model in curvature coordinate system consistent with observational data

Jitendra Kumar^{a,1}, Puja Bharti^{b,1}

¹Central University of Jharkhand, Cheri-Manatu, Ranchi, India.

Received: date / Accepted: date

Abstract

This paper investigates a spherically symmetric compact relativistic body with isotropic pressure profiles within the framework of general relativity. In order to solve the Einstein's field equations, we have considered the Vaidya–Tikekar type metric potential, which depends upon parameter K . We have presented a charged perfect fluid model, considering $K \notin [0, 1]$, which represent compact stars like Her X-1, 4U 1538-52, SAX J1808.4-3658, LMC X-4, SMC X-4, EXO 1785-248, Cen X-3 and Cyg X-2, to an excellent degree of accuracy. We have investigated the physical features such as the energy conditions, velocity of sound, surface redshift, adiabatic index of the model in detail and shown that our model obeys all the physical requirements for a realistic stellar model. Using the Tolman–Oppenheimer–Volkoff equations, we have explored the hydrostatic equilibrium and the stability of the compact objects. This model also fulfils the Harrison–Zeldovich–Novikov stability criterion. The results obtained in this paper can be used in analyzing other isotropic compact objects.

Key words: Compact stars; General Relativity; Pressure isotropy; Field equations; Perfect fluid, Exact solutions.

^ae-mail: jitendark@gmail.com

^be-mail: pujabharti06@gmail.com

1 Introduction

General relativity is a great medium for understanding and exploring the gravitational system. Ultra-compact objects like pulsars, neutron stars and black holes have helped scientists to look for exact solutions of the Einstein field equations by modelling physical objects based on observational data, rather than by using mere mathematical excursions. Several theoretical investigations, laboratory experiments and observational tests have been performed during the previous couple of decades. But, it has been difficult to obtain a reliable description of dense compact object. The observational data forming compact stars might be able to provide information about the largest uncertainties in nuclear physics that rely heavily on the equations of state (EoS) at nuclear and supranuclear densities. We might achieve this by estimating their mass and radius which depends on EoS.

The first solution of the Einstein field equations describing a self-gravitating, bounded object was obtained by Schwarzschild [1] about a century ago. The Schwarzschild interior solution describes a uniform density sphere. It was the first approximation in describing the gravitational field of a static, spherically symmetric object. Although this model is not realistic as the propagation speed within the object exceeds the speed of light, the efforts put by Schwarzschild motivated the researchers to search for exact solutions of the Einstein field equations describing self-gravitating objects. As a result, we have a large number of exact solutions of the field equations describing an outsized number of stellar objects. The analysis of available exact solutions indicates that many of them are unable to describe physically realizable stellar structures [2]. While few of these solutions are only valid in some region of the object, some other solutions display unphysical behaviour in the density and pressure profiles.

A large number of currently existing exact solutions were obtained through various assumptions on the space-time geometry and/or matter content inside the compact object [3]. Spherical symmetry is the most common assumption, while modelling static stars. But, there is more freedom in choosing the matter content of the stellar fluid. History tells us that researchers have already worked with perfect fluids, charged interiors, pressure anisotropy, bulk viscosity and scalar fields. Developments in cosmology, inspired the researchers to model stellar structures which includes dark energy, dark matter and phantom energy [4, 5].

There is no doubt that an astrophysical structure is not composed of a perfect fluid. However, we may consider relativistic static perfect fluid spheres as first approximation to compact star models. The perfect fluid model necessarily requires that the pressure inside a star should be isotropic, i.e., it should have equal radial (p_r) and tangential (p_t) pressures.

Recent developments in cosmological survey have made us understand the origin and distribution of matter and evolution of compact objects in the Universe. We can measure some of their properties like mass, rotation frequency and emission of radiation. Whereas, measurement of parameters which determines the nature of compact stars is still a great challenge. Properties such as internal composition, mass and radius, which are not directly linked to observations, requires theoretical models. These theoretical mass and radius are determined by solving the hydrostatic equilibrium equation which convey the equilibrium between gravitational force and pressure. Limited knowledge of nuclear EoS leads to unpredictability of Mass-radius relation. This limits the mass of compact stars. As per Buchdahl [9], for a regular fluid sphere with a non increasing mass density, the ratio of its gravitational mass M to that of coordinate radius R satisfies $\frac{M}{R} < \sim \frac{4}{9}$. This constraint arises from the condition that, to prevent gravitational collapse, isotropic pressure does not become infinity at the center of the sphere. In general relativity, the equilibrium of a spherical object is

described by the Tolman–Oppenheimer–Volkoff (TOV) equations, and the equation of state is required for its completeness.

To determine the structure of a compact star, the most common route is to specify an equation of state and then solve the Einstein field equations. Traditionally, this approach has been proved beneficial while using the law of energy conservation in the form of the TOV equation or the equation of hydrodynamical equilibrium.

The equation of state of a compact star is not very clear yet. If one starts with EoS, she generally lands into numerical methods leading to graphical results which lacks in the analysis of local properties of the matter close to the centre of such relativistic stars. Therefore, most researchers prefer to obtain exact solutions of the concerned Einstein's field equations using ad-hoc methods such as assuming one of the metric potential. The remaining metric potential is obtained using isotropic conditions for perfect fluid. After this, the physical quantities including pressure, energy density, velocity of sound and adiabatic indices are examined for the reality as well as stability conditions inside the fluid sphere. Examples of some remarkable perfect fluid solutions by assuming metric potential g_{11} can be found in [1, 6–17].

To find the exact solution of the Einstein–Maxwell field equations, Komathiraj and Maharaj [18] have used Vaidya and Tikekar ansatz [14] for metric potential with a specified form of electric field intensity. Bijalwan and Gupta [19, 20] have obtained a charged perfect fluid model with generalized electric intensity for all $K \notin (0, 1)$. By extending this work, Kumar and Gupta [26, 27] obtained another solution for $K \in (0, 1)$. Using this approach, a large number of solutions have been obtained in [21–23, 25]. Recently, Kumar et. al. [30, 36] has obtained perfect fluid charged analogues models with generalized electric intensity for $K \in (0, 1)$. Some other references of solutions using Buchdahl (Vaidya-Tikekar) ansatz (for K in $[0, 1]$, > 1 or < 0) can be found in [24, 33–35].

In this paper, we are going to use a physically viable Vaidya and Tikekar [14] metric potential to obtain a closed-form solution of the Einstein field equations for a spherically symmetric isotropic matter distribution. We will use this solution to develop feasible models for compact stars with some standard observed mass and radius as proposed in [32, 36]. To find out the model parameters, we will utilize the boundary conditions, which says that interior spacetime metric matches the exterior Schwarzschild metric at surface and radial pressure is zero across the boundary. Due to the complexity of the solution, we will use graphical approach to verify if the matter variables of the model satisfy criteria for realistic star.

This paper has been organized as mentioned below:

In Sect. 2, the Einstein field equations for the isotropic system of the compact object has been presented. In Sect. 3, by assuming the Vaidya-Tikekar metric potential, the relevant field equations has been solved to develop a new model. In Sect. 4, an analytical and graphical representations has been performed to check the physical acceptability and stability of the model. For this we have used recent measurements of mass and radius of stars SMC X-1, Her X-1, 4U 1538-52, SAX J1808.4-3658, LMC X-4, EXO 1785-248 and Cyg X-2. Finally, Sect. 5 is devoted to conclusion.

2 Metric and the Field equations

Let us consider the line element to describe the static and spherically symmetric stellar system in curvature coordinates $(x^i) = (t, r, \theta, \phi)$

$$ds^2 = e^{v(r)} dt^2 - e^{\lambda(r)} dr^2 - r^2(d\theta^2 + \sin^2\theta d\phi^2), \quad (1)$$

where the metric potentials $v(r)$ and $\lambda(r)$ are arbitrary functions of radial coordinate r . These potentials plays a key role in determining the surface redshift and gravitational mass function respectively.

The Einstein-Maxwell field equations for obtaining the hydrostatic stellar structure of the charged sphere can be written as

$$-\kappa(T_j^i + E_j^i) = R_j^i - \frac{1}{2}R\delta_j^i = G_j^i, \quad (2)$$

where $\kappa = \frac{8\pi G}{c^4}$, G here stands for gravitational constant and c is the speed of light, R_j^i and R represent Ricci Tensor and Ricci Scalar respectively. Throughout the discussion we will take $G = c = 1$, as geometrized units. Since we are assuming that matter within the star is a charged perfect fluid, the corresponding energy-momentum tensor T_j^i and electromagnetic field tensor E_j^i will be

$$T_j^i = (\rho + p)v^i v_j - p\delta_j^i \quad (3)$$

and

$$E_j^i = \frac{1}{4\pi}(-F^{im}F_{jm} + \frac{1}{4}F^{mn}F_{mn}), \quad (4)$$

where, $\rho(r)$ is the energy density, $p(r)$ is the isotropic pressure, F_{ij} is anti-symmetric electromagnetic field strength tensor defined as $F_{ij} = \frac{\partial A_j}{\partial x_i} - \frac{\partial A_i}{\partial x_j}$ which satisfies Maxwells equations,

$$F_{ik,j} + F_{kj,i} + F_{ji,k} = 0 \text{ and } [\sqrt{-g}F^{ik}]_{,k} = 4\pi J^i \sqrt{-g}$$

Here $A_j = (\phi(r), 0, 0, 0)$ is the potential and J^i is the electromagnetic current vector defined as $J^i = \frac{\sigma}{\sqrt{g_{44}}} \frac{dx^i}{dx^4} = \sigma v^i$, where $\sigma = e^{(v/2)} J^0$ represents the charge density, g is the determinant of the metric g_{ij} which is defined by $g = -e^{v+\lambda} r^4 \sin^2\theta$ and J^0 is the only non-vanishing component of the electromagnetic current J^i for the static spherically symmetric stellar system. Since the field is static, we have $v = (0, 0, 0, \frac{1}{\sqrt{g_{44}}})$.

Also, the total charge within a sphere of radius r is given by

$$q(r) = r^2 E(r) = 4\pi \int_0^r J^0 r^2 e^{(v+\lambda)/2} dr, \quad (5)$$

where, $E(r)$ is the intensity of the electric field.

Thus, for the spherically symmetric metric of Eq. (1) the Einstein-Maxwell field equation (2) provides the following relationship [28]:

$$\frac{\lambda'}{r} e^{-\lambda} + \frac{1 - e^{-\lambda}}{r^2} = c^2 \kappa \rho + \frac{q^2}{r^4}, \quad (6)$$

$$\frac{v'}{r} e^{-\lambda} - \frac{1 - e^{-\lambda}}{r^2} = \kappa p - \frac{q^2}{r^4}, \quad (7)$$

$$\left(\frac{v''}{2} - \frac{\lambda' v'}{4} + \frac{v'^2}{4} + \frac{v' - \lambda'}{2r} \right) e^{-\lambda} = \kappa p + \frac{q^2}{r^4} \quad (8)$$

Here prime denotes differentiation with respect to r . Using Eqs. (7) and (8), we can obtain

$$\left(\frac{v''}{2} - \frac{\lambda' v'}{4} + \frac{v'^2}{4} - \frac{v' + \lambda'}{2r} - \frac{1}{r^2} \right) e^{-\lambda} + \frac{1}{r^2} = \frac{2q^2}{r^4} \quad (9)$$

We can get the definition of charged density σ by substituting this value in eq. (5).

Let us consider $m(r)$ to be the mass function for an electrically charged fluid sphere, given as [37]

$$m(r) = \frac{\kappa}{2} \int_0^r (c^2 \rho r^2 + r \sigma q e^{\lambda/2}) dr = \frac{r}{2} \left(1 - e^{-\lambda} + \frac{q^2}{r^2} \right). \quad (10)$$

Consider $r = R$ as the outer boundary of the fluid sphere. The unique exterior metric for a spherically symmetric charged distribution of matter is the Reissner-Nördstro metric

$$ds^2 = \left(1 - \frac{2M}{r} + \frac{Q^2}{r^2} \right) dt^2 - \left(1 - \frac{2M}{r} + \frac{Q^2}{r^2} \right)^{-1} dr^2 - r^2 (d\theta^2 + \sin^2 \theta d\phi^2) \quad (11)$$

where, $M = m(R)$, is total gravitational mass and $Q = q(R)$ is total electric charge.

3 Exact solutions of the models for isotropic stars

We are going to uncover the solutions to Einstein's field equations for isotropic fluid matter. To achieve this, we have to solve 3 equations (6,7& 9) for 5 unknown functions. Let's specify two variables a priori to solve these equations analytically.

Let's consider the metric ansatz, given by Vaidya and Tikekar [14]

$$e^\lambda = \frac{K(1+Cr^2)}{K+Cr^2}, \quad (12)$$

and a new variable as

$$e^\nu = Z^2(r) \quad (13)$$

where C and K are some constant parameters. This choice of metric potential provides a singularity free solution at $r = 0$ and $e^\lambda(0) = 1$. Vaidya and Tikekar [14] had considered this metric potential to study spheroidal spacetimes governing the behavior of superdense stars. Several works utilizing this form of metric potential can be found in literature [29, 30, 32].

In order to get the exact solutions more efficiently, we will use the above substitutions, so that we can transform the field equations to an equivalent form as,

$$c^2 \kappa \rho + \frac{q^2}{r^4} = \frac{C(K-1)(3+Cr^2)}{K(1+Cr^2)^2} \quad (14)$$

$$\kappa p - \frac{q^2}{r^4} = \frac{K+Cr^2}{K(1+Cr^2)} \frac{2Z'}{rZ} + \frac{C(1-K)}{K(1+Cr^2)} \quad (15)$$

and

$$\frac{d^2 Z}{dr^2} - \left[\frac{K+2KCr^2+C^2r^4}{r(1+Cr^2)(K+Cr^2)} \right] \frac{dZ}{dr} + \left[\frac{C^2r^2(K-1)}{(K+Cr^2)(1+Cr^2)} - \frac{2Kq^2(1+Cr^2)}{r^4(K+Cr^2)} \right] Z = 0 \quad (16)$$

Here we are considering the charged perfect fluid distribution represented by metric (1) when $K \notin [0, 1]$, i.e., for $K < 0$ and $K > 1$.

To get a convenient form of the above equations let's introduce the transformation

$$X = \sqrt{\frac{K + Cr^2}{K - 1}} \quad (17)$$

where, $0 < C < \frac{|K|}{R^2}$ is a parameter, which characterizes the geometry of star. Substituting the value of X into eq. (16), we get,

$$\frac{d^2 Z}{dX^2} - \frac{X}{X^2 - 1} \frac{dZ}{dX} + (K - 1) \left[\frac{1}{X^2 - 1} - \frac{2K(1 + Cr^2)q^2}{C^2 r^6} \right] Z \quad (18)$$

It is obvious from eq. (17) that when K is negative X is less than 1 and when $K > 1$, we get $X > 1$.

Let's use the transformation

$$Z = (1 - X^2)^{1/4} Y \text{ when } K < 0 \text{ \& } Z = (X^2 - 1)^{1/4} Y \text{ when } K > 1 \quad (19)$$

to convert eq. (18) into the normal form

$$\frac{d^2 Y}{dX^2} + \phi Y = 0, \quad (20)$$

where,

$$\phi = \frac{1}{1 - X^2} \left[1 - K + \frac{2Kq^2(1 + Cr^2)^2}{C^2 r^6} + \frac{3X^2 + 2}{4(X^2 - 1)} \right] \quad (21)$$

It is difficult to solve the second order differential equation (20) using standard techniques. In order to solve this differential equation, let's take

$$\phi = -\frac{2a_1}{X^2(a_1 + a_2 X)} \quad (22)$$

where, $a_1, a_2 \in \mathbb{R}$ such that a_1 is non-zero.

We have made this choice for ϕ , as it will later become evident that it simplifies the analysis. For the stars which we have considered here, such a choice gives physically viable electric field intensity.

Putting this value of ϕ from eq. (22) to eq. (20), the resulting differential equation becomes

$$X^2(a_1 + a_2 X) \frac{d^2 Y}{dX^2} - 2a_1 Y = 0 \quad (23)$$

It's solution can be given by

$$Y = \frac{a_1 + a_2 X}{X} \left[A_1 \frac{a_1}{a_2^3} S(X) + A_2 \right] \quad (24)$$

where, A_1 and A_2 are arbitrary constants and

$$S(X) = \frac{\sec^2 \left(\tan^{-1} \sqrt{\frac{a_2 X}{a_1}} \right)}{2} - \frac{\cos^2 \left(\tan^{-1} \sqrt{\frac{a_2 X}{a_1}} \right)}{2} + 2 \log \left| \cos \left(\tan^{-1} \sqrt{\frac{a_2 X}{a_1}} \right) \right| \quad (25)$$

Using eqs. (19) and (24) we get the value of Z as,

$$\begin{aligned} Z &= A_1(1-X^2)^{1/4} \frac{a_1+a_2X}{X} \left[\frac{a_1}{a_2^3} S(X) + \frac{A_2}{A_1} \right], \text{ when } K < 0 \\ Z &= A_1(X^2-1)^{1/4} \frac{a_1+a_2X}{X} \left[\frac{a_1}{a_2^3} S(X) + \frac{A_2}{A_1} \right], \text{ when } K > 1 \end{aligned} \quad (26)$$

We will show in the next section that the obtained metric function $Z = e^{v/2}$ is finite, free from singularity at centre with $v'(0) = 0$ and monotonically increasing throughout the stellar interior, i.e., it satisfies the prerequisites for any physically acceptable model provided by Lake [48]. This function will act as the second necessary condition which we have imposed to generate the model along with the assumption (12).

Now, let's obtain the expression for electric charge, energy density and pressure.

On comparing eqs. (21) and (22), we get the definition of electric field intensity as

$$E^2 = \frac{q^2}{r^4} = \frac{C^2 r^2}{2K(1+Cr^2)^2} \left[\frac{5}{4} \frac{1}{(1-X^2)} - \frac{2a_1}{X^2(a_1+a_2X)} (1-X^2) + K - \frac{7}{4} \right] \quad (27)$$

Putting eqs. (27) and (26) into eqs. (14) and (15) respectively, we obtain the expressions for energy density and pressure as:

$$c^2 \kappa \rho = \frac{C(K-1)(3+Cr^2)}{K(1+Cr^2)^2} - \frac{C^2 r^2}{2K(1+Cr^2)^2} \left[\frac{5}{4(1-X^2)} - \frac{2a_1(1-X^2)}{X^2(a_1+a_2X)} + K - \frac{7}{4} \right] \quad (28)$$

$$\kappa p = \frac{CX^2}{K(X^2-1)} \left[\frac{P_1 P_2 + P_3 P_4}{P_2 P_5} \right] - \frac{C}{K(X^2-1)} + \frac{C^2 r^2}{2K(1+Cr^2)^2} \left[\frac{5}{4(1-X^2)} - \frac{2a_1(1-X^2)}{X^2(a_1+a_2X)} + K - \frac{7}{4} \right] \quad (29)$$

From eqs. (28) and (29), gradient of density and pressure can be obtained as,

$$c^2 \kappa \frac{d\rho}{dr} = C^2 r [D_6 - D_7 - D_8] \quad (30)$$

$$\kappa \frac{dp}{dr} = C^2 r \left[\frac{X^2}{K(X^2-1)} \frac{D}{P_2 P_5} + \frac{2}{K(1-K)(X^2-1)^2} \left(\frac{P_1 P_2 + P_3 P_4}{P_2 P_5} - 1 \right) + D_7 + D_8 \right] \quad (31)$$

respectively.

See Appendix A for values of P_i ($1 \leq i \leq 5$), D and D_j ($1 \leq j \leq 8$).

4 Physical features and stability analysis of the model

In this section, we are going to perform some analytical calculations to ensure that this model is obeying essential physics for a stellar structure throughout the interior and outer surface. We will do the stability analysis of the model by studying general physical properties and plotting several figures for some of the compact star candidates. The solutions found in this paper might be useful in study of relativistic compact stellar objects.

4.1 Boundary Conditions

To explore the boundary conditions, we are going to use the fact that all astrophysical objects are immersed in vacuum or almost vacuum space-time. Also, the interior metric (1) joins smoothly at the surface of spheres ($r = R$) to the exterior metric (11). In order to match smoothly on the boundary surface $r = R$, we will impose the boundary conditions which are equivalent to the following two conditions:

$$e^{v(R)} = Z^2(R) = 1 - \frac{2M}{R} + \frac{Q^2}{R^2}, \text{ \& } e^{-\lambda(R)} = 1 - \frac{2M}{R} + \frac{Q^2}{R^2}, \quad (32)$$

and

$$P(R) = 0 \quad (33)$$

where, $Q = q(R)$. Using these boundary conditions (32,33), we can easily obtain the constants A_1 and A_2 (see Appendix B).

For a given radius R , we can determine the total mass M of the star and vice-versa. Keeping in mind the constraints on the mass-radius ratio $\left(\frac{2M}{R} \leq \frac{8}{9}\right)$ [9, 38], we have demonstrated that for some particular values of the parameters, we can generate specific mass and radius of some well known pulsars. In this process we have used true values of c and G at appropriate places. Some of such possibilities are tabulated in Table 1.

Table 1 The approximate values of the masses M , radii R , and the constants a_1 , a_2 , C and K for the compact stars

Compact Star	a_1	a_2	$C(/km^2)$	K	M/M_\odot	$R(km)$	M/R
Her X-1 [32]	0.7	2.6	0.003078799	-1.313519	0.85	8.1	0.15475
4U 1538-52 [32]	0.07	4.6	0.003393997	-1.208442	0.87	7.866	0.16314
SAX J1808.4-3658 [32]	0.07	4.58	0.003369272	-1.18123	0.9	7.951	0.16696
LMC X-4 [36]	0.07	2.6	0.003192728	-1.02362	1.04	8.301	0.18479
SMC X-4 [32]	0.07	2.6	0.003077453	-0.944478	1.29	8.831	0.21546
EXO 1785-248 [32]	0.7	2.6	0.003448064	-1.132761	1.3	8.849	0.21669
Cen X-3 [36]	0.5	1.2	0.003561436	-1.150118	1.49	9.178	0.23945
Cyg X-2 [36]	0.07	4.1	4.213965167	2.106839	1.71	8.313	0.303519

Table 2 Numerical values of surface charge (q_s), central density (ρ_0), surface density (ρ_s), central pressure (p_0) and surface redshift (z_s) of compact star candidates.

Compact star	$q_s(C)$	$\rho_0(g/cc)$	$\rho_s(g/cc)$	$p_0(Pa)$	z
Her X-1	1.10029×10^{20}	8.72888×10^{14}	6.33727×10^{14}	4.26198×10^{33}	0.191824
4U 1538-52	8.75131×10^{19}	9.9841×10^{14}	7.21771×10^{14}	7.40078×10^{33}	0.210164
SAX J1808.4-3658	9.11424×10^{19}	1.00147×10^{15}	7.20756×10^{14}	7.62543×10^{33}	0.21649
LMC X-4	1.10765×10^{20}	1.01599×10^{15}	7.22473×10^{14}	8.53183×10^{33}	0.246591
SMC X-4	1.42547×10^{20}	1.06235×10^{15}	7.23379×10^{14}	1.09311×10^{34}	0.303832
EXO 1785-248	1.87705×10^{20}	1.04499×10^{15}	6.83534×10^{14}	6.32214×10^{33}	0.291296
Cen X-3	2.33211×10^{20}	1.07173×10^{15}	6.67313×10^{14}	5.29925×10^{33}	0.326182
Cyg X-2	2.79936×10^{20}	3.56354×10^{17}	3.44725×10^{14}	9.36725×10^{36}	0.448752

4.2 Regularity and Reality Conditions

It is clear from fig (1) and (2) that the obtained metric potentials e^λ and e^ν are free from physical and geometrical singularities. Additionally, they are finite and monotonically increasing throughout the stellar interior. Thus, the behavior of metric functions is consistent with the requirements.

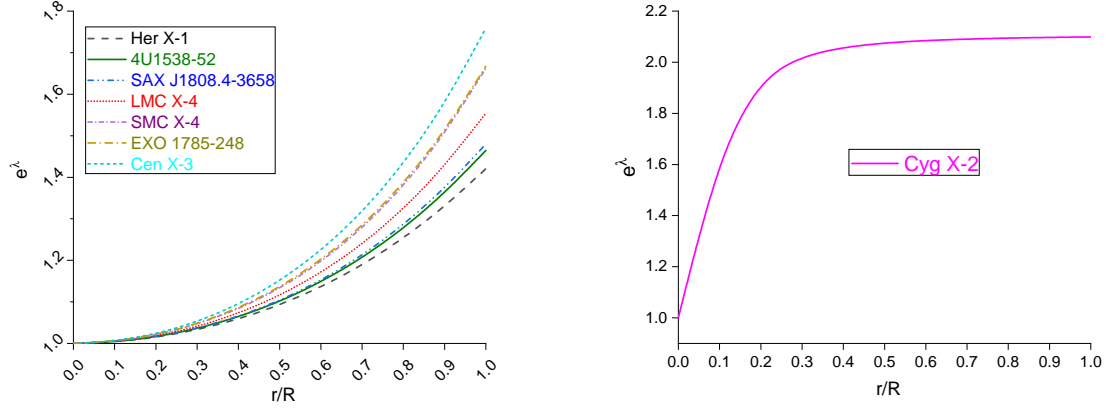


Fig. 1 Behavior of e^λ within the stellar configuration of star candidates Her X-1, 4U 1538-52, SAX J1808.4-3658, LMC X-4, SMC X-4, EXO 1785-248, Cen X-3 ($K < 0$) and Cyg X-2 ($K > 1$).

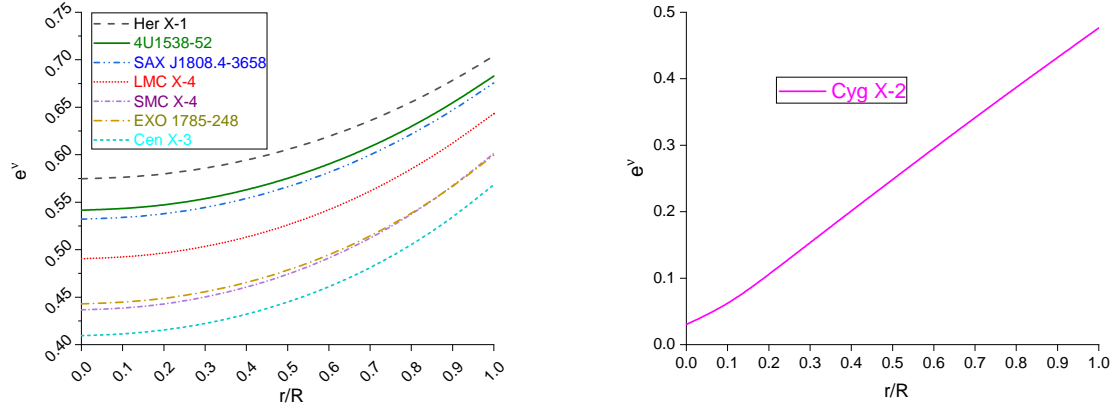


Fig. 2 Behavior of e^ν within the stellar configuration of star candidates Her X-1, 4U 1538-52, SAX J1808.4-3658, LMC X-4, SMC X-4, EXO 1785-248, Cen X-3 ($K < 0$) and Cyg X-2 ($K > 1$).

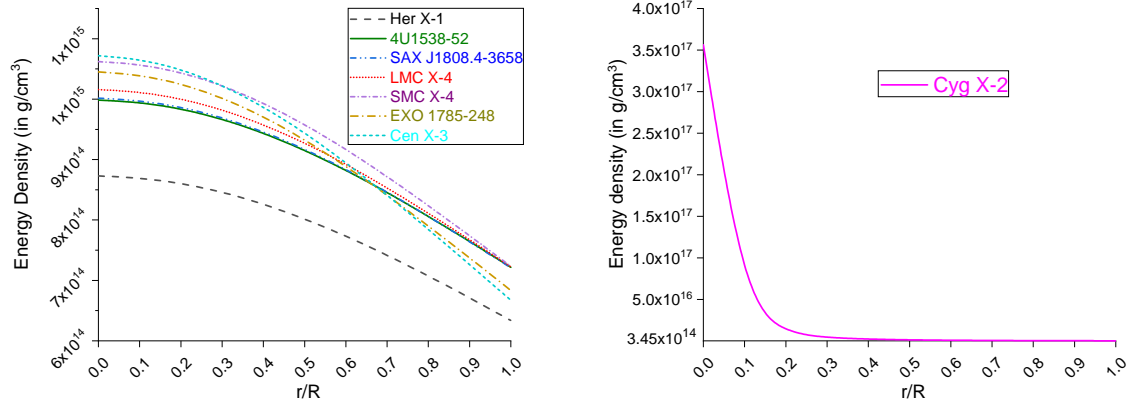


Fig. 3 Variation of density with respect to fractional radius (r/R) for star candidates Her X-1, 4U 1538-52, SAX J1808.4-3658, LMC X-4, SMC X-4, EXO 1785-248, Cen X-3 ($K < 0$) and Cyg X-2 ($K > 1$).

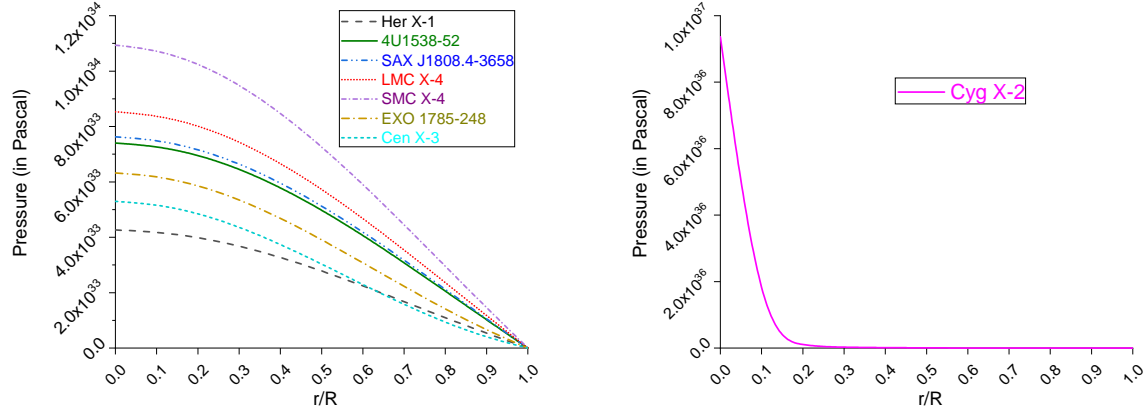


Fig. 4 Variation of pressure with respect to fractional radius (r/R) for star candidates Her X-1, 4U 1538-52, SAX J1808.4-3658, LMC X-4, SMC X-4, EXO 1785-248, Cen X-3 ($K < 0$) and Cyg X-2 ($K > 1$).

For physical feasibility of the model it is also required that

- the energy density is positive definite and its gradient is negative everywhere within the radius.
- for an isotropic fluid distribution pressure is positive definite and the pressure gradient is negative within the stellar interior.

Graphs in Fig. (3) and (4) indicate that the energy density is positive with a maximum value at the centre and the pressure is finite and vanishes at the boundaries for each considered star candidates. Also, both pressure as well as density are monotonically decreasing in nature towards the surface of star. We have taken the same values of the constants as mentioned in Table 1.

4.3 Electric charge

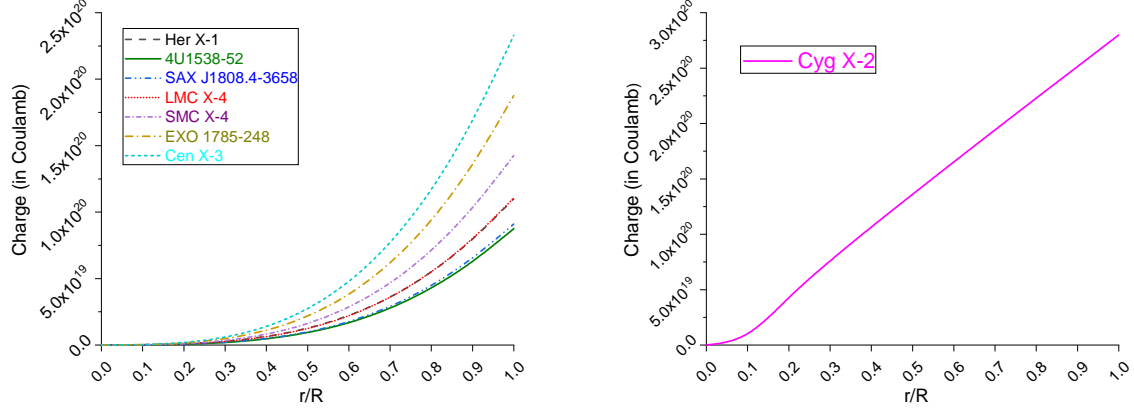


Fig. 5 Variation of charge with respect to fractional radius (r/R) for star candidates Her X-1, 4U 1538-52, SAX J1808.4-3658, LMC X-4, SMC X-4, EXO 1785-248, Cen X-3 ($K < 0$) and Cyg X-2 ($K > 1$).

The fig (5), clearly states that the electric field given by eq. (27) is positive and increasing towards the surface for each star candidate. Along with this, the charge at centre is zero and attains its maximum value at the boundary.

Ray et al. [49] have demonstrated that the global balance of the forces allows a huge charge (10^{20}C) to be available inside a compact star. Referring to the Table 2, we can say that, in this model the net charge is effective to balance the mechanism of the force.

4.4 Charge density

Charge density is the amount of electric charge per unit volume. Differentiating eq. (5) with respect to r we obtain the expression for charge density as,

$$\sigma = \frac{e^{-\lambda/2}}{4\pi r^2} \frac{dq}{dr} \quad (34)$$

Figure 6 shows that the proper charge density is finite at $r = 0$, regular in the interior, and evolves as a decreasing function throughout for each compact star candidates.

4.5 Mass–radius relation and compactness factor

By plugging Eqs. (12) and (27) into Eq. (10), eventually we get

$$m(r) = \frac{(K-1)Cr^3}{2K(1+Cr^2)} + \frac{C^2r^5}{4K(1+Cr^2)^2} \left[\frac{5}{4} \frac{1}{(1-X^2)} - \frac{2a_1}{X^2(a_1+a_2X)} (1-X^2) \frac{7}{4} \right]. \quad (35)$$

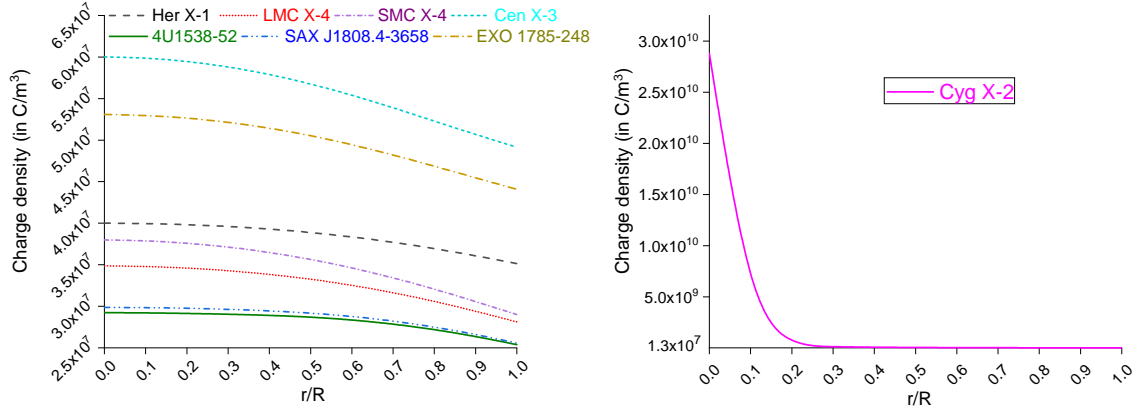


Fig. 6 Variations of charge density with respect to fractional radius (r/R) for star candidates Her X-1, 4U 1538-52, SAX J1808.4-3658, LMC X-4, SMC X-4, EXO 1785-248, Cen X-3 ($K < 0$) and Cyg X-2 ($K > 1$).

In Fig. 7, the mass function is plotted against the radius and the profile indicates an increasing function with increase of radius. For physically viable models, the ratio of the mass to that of radius of a compact star model cannot be arbitrarily large. According to Buchdahl [9], the ratio of mass to the radius for a perfect fluid compact star should satisfy the inequality $\frac{2M}{R} < \frac{8}{9}$. The compactness factor $\mu(r) = \frac{m(r)}{r}$ can be computed as,

$$\mu(r) = \frac{(K-1)Cr^2}{2K(1+Cr^2)} + \frac{C^2r^4}{4K(1+Cr^2)^2} \left[\frac{5}{4} \frac{1}{(1-X^2)} - \frac{2a_1}{X^2(a_1+a_2X)} (1-X^2) \frac{7}{4} \right]. \quad (36)$$

The compactness factor is plotted in Fig. 8. We can see in Table 1 that for each compact

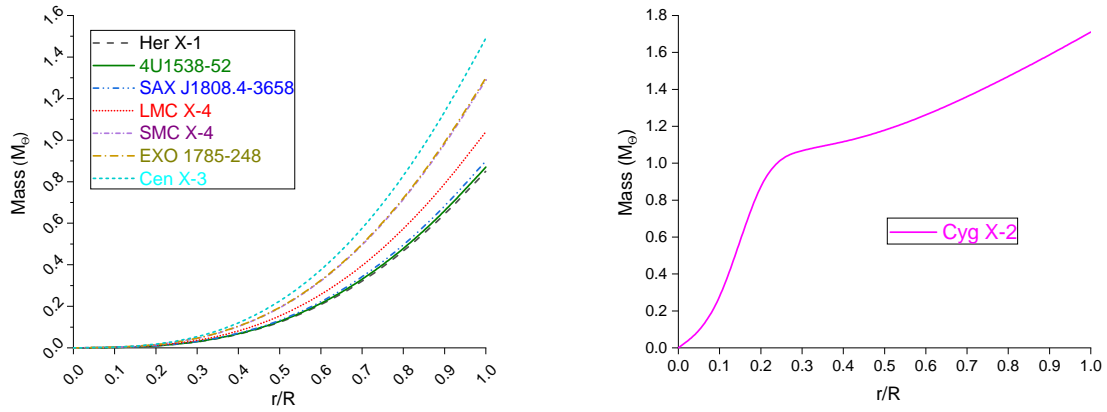


Fig. 7 Variation of mass with respect to fractional radius (r/R) for star candidates Her X-1, 4U 1538-52, SAX J1808.4-3658, LMC X-4, SMC X-4, EXO 1785-248, Cen X-3 ($K < 0$) and Cyg X-2 ($K > 1$).

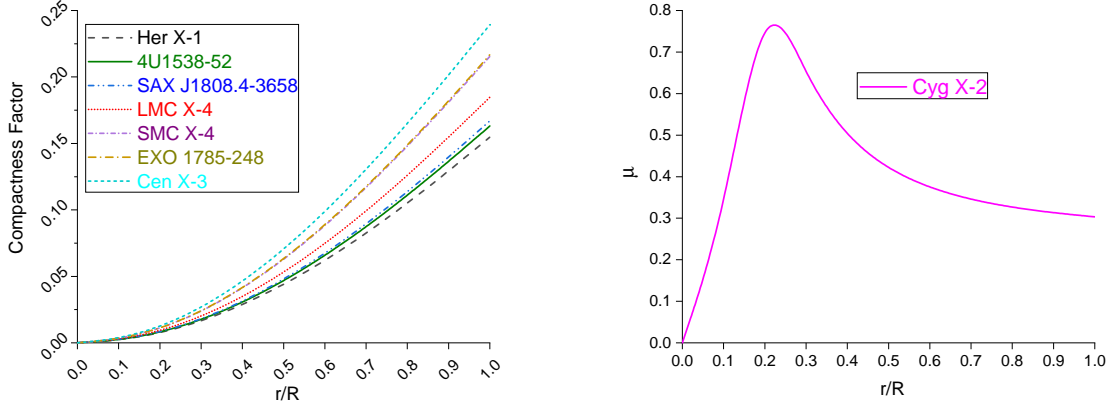


Fig. 8 Compactness factor with respect to fractional radius (r/R) for star candidates Her X-1, 4U 1538-52, SAX J1808.4-3658, LMC X-4, SMC X-4, EXO 1785-248, Cen X-3 ($K < 0$) and Cyg X-2 ($K > 1$).

star candidate we have considered here, the value of μ is consistent with the condition of Buchdahl. However, Böhmer and Harko [39] have given the generalized expression of lower bound for a charged compact object as follows:

$$\frac{Q^4 + 18R^2Q^2}{12R^4 + R^2Q^2} \leq \frac{2M}{R} \quad (37)$$

Subsequently, Andreasson [40] showed that, for a charged sphere, the model must satisfy the following inequality

$$\sqrt{M} \leq \frac{\sqrt{R}}{3} + \sqrt{\frac{R^2 + 3Q^2}{9R}} \quad (38)$$

We, therefore, conclude from the above two conditions that $\frac{2M}{R}$ must satisfy the following inequality:

$$\frac{Q^2}{R^2} \left(\frac{Q^2 + 18R^2}{12R^2 + Q^2} \right) \leq \frac{2M}{R} \leq \frac{2}{R} \left[\frac{\sqrt{R}}{3} + \sqrt{\frac{R^2 + 3Q^2}{9R}} \right]^2. \quad (39)$$

Using eq. (39), we have obtained the ranges for compactness factor in Table 3. We can

Table 3 Upper and lower bound of μ for the compact star candidates.

Compact Star	Her X-1	4U 1538-52	SAX J1808.4-3658	LMC X-4	SMC X-4	EXO 1785-248	Cen X-3	Cyg X-2
Lower bound	0.010176926	0.006827579	0.007248024	0.00982036	0.014368244	0.02480304	0.035576893	0.062467518
Upper bound	0.453448858	0.450494487	0.450865833	0.453134756	0.457133708	0.466250717	0.475582871	0.498546049

observe from Table 1 and Table 3 that the value of μ , for the considered compact star candidates, lie in this range. Thus, μ for each compact star candidate is consistent with the condition (39) for a stable configuration.

4.6 Gravitational redshift and Surface redshift

Let's consider the gravitational redshift z_g of compact objects with help of the definition, $z_g = \frac{\lambda_0 - \lambda_e}{\lambda_e}$, where λ_0 is the observed wavelength and λ_e is the emitted wavelength at the surface of a non-rotating star. Thus, the gravitational redshift from the surface of the star, as measured by a distant observer, is given by

$$z = \frac{1}{\sqrt{|e^{v(R)}|}} - 1 = \left(1 - \frac{2M}{R} + \frac{Q^2}{R^2}\right)^{-1/2} - 1 \quad (40)$$

Gravitational redshift is a phenomenon in which electromagnetic waves or photons seem to lose energy when it climbs out of a gravitational well. The surface redshift depends on the surface gravity, i.e., on the overall mass and radius of stellar object. The gravitational (interior) redshift $z_g(r)$ and surface redshift $z_s(r)$ are defined as,

$$z_g(r) = \frac{1}{\sqrt{|e^{v(r)}|}} - 1 \quad (41)$$

$$z_s(r) = \frac{1}{\sqrt{1 - 2\mu + \frac{q^2}{r^2}}} - 1 \quad (42)$$

If a photon comes out from center to surface, it has to travel a denser region and longer path, which leads to more dispersion and a great loss of energy. Whereas, when a photon comes out from near the surface, it has to travel a comparatively less denser region and shorter path, therefore, it goes through less dispersion and less energy loss takes place. Hence, the interior redshift is minimum at the surface and maximum at the center.

As radius slightly increases with increase in mass resulting into more surface gravity, the surface redshift is maximum at the surface and decreases towards the center. Moreover, at the surface of stars, $z_s(R) = z_g(R) = z$, implying that minimum value of interior redshift is the maximum for surface redshift.

To explore the behaviour of the redshifts, we have provided its graphical representation in Fig. 9. We can see through figure that the redshifts has no singularity throughout its configuration.

For an isotropic star a constraint on the gravitational redshift for perfect fluid spheres is given by $z_s < 2$ [9, 42]. As can be seen in Table 2, for the constants mentioned in Table 1, surface redshift of the star candidates have values less than 2.

4.7 Causality Condition

Now, we are going to analyse the speed of sound propagation v_s^2 , which is given by

$$v_s^2 = \frac{dp}{d\rho} = \frac{\frac{X^2}{K(X^2-1)} \frac{D}{P_2 P_3} + \frac{2}{K(1-K)(X^2-1)^2} \left(\frac{P_1 P_2 + P_3 P_4}{P_2 P_3} - 1 \right) + D_7 + D_8}{D_6 - D_7 - D_8} \quad (43)$$

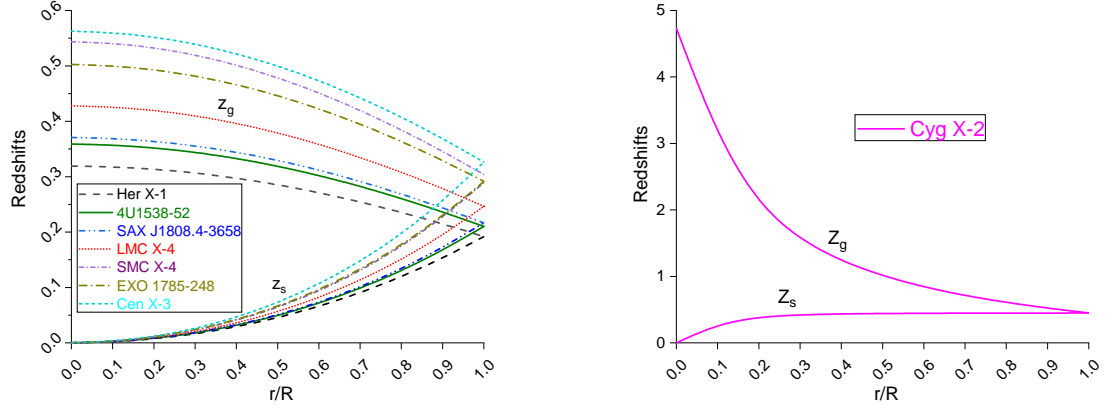


Fig. 9 Variation of redshift with respect to fractional radius (r/R) for star candidates Her X-1, 4U 1538-52, SAX J1808.4-3658, LMC X-4, SMC X-4, EXO 1785-248, Cen X-3 ($K1$).

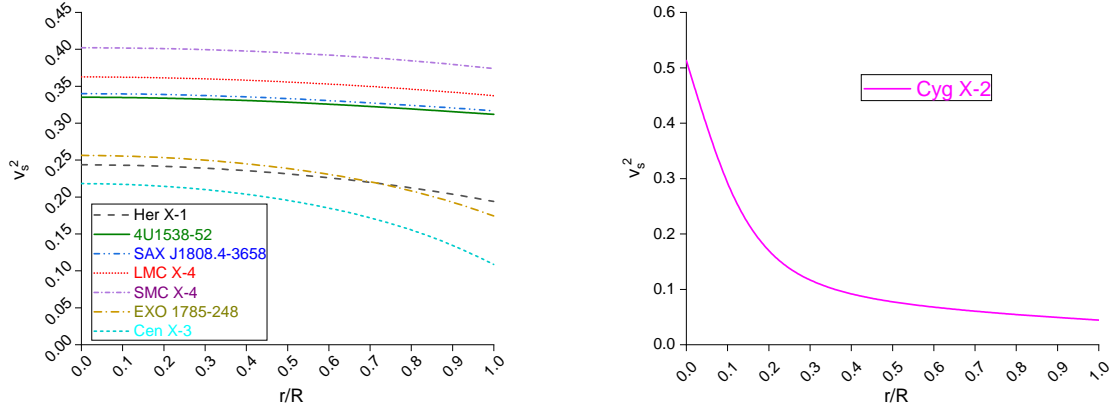


Fig. 10 Variation of velocity of sound of compact star candidates Her X-1, 4U 1538-52, SAX J1808.4-3658, LMC X-4, SMC X-4, EXO 1785-248, Cen X-3 ($K < 0$) and Cyg X-2 ($K > 1$) with respect to fractional radius (r/R).

Naturally the velocity of sound does not exceed the velocity of light. Thus, the sound speed must have value less than 1, as we have taken $c = 1$. For a physically acceptable isotropic fluid distribution, the causality condition, i.e., $0 \leq v_s^2 \leq 1$, must be satisfied to achieve a stable equilibrium. It was stated by Canuto [45] that for an ultra-high distribution of matter, the speed of sound should decrease monotonically towards the surface of the star. We have shown in Fig. (10) that, for our charged isotropic model, the speed of sound remains less than the speed of light and for each star candidate, it decreases with increase in r .

4.8 Equation of state

The term "Equation of state (EoS)" means a function $p(\rho)$, which establish a relation between the pressure p and energy density ρ . Lets consider that the pressure of the charged fluid sphere is related with their energy density, by a parameter ω via the EoS, $p = \omega\rho$, which is given by

$$\omega = \frac{\frac{X^2}{X^2-1} \left[\frac{P_1 P_2 + P_3 P_4}{P_2 P_5} \right] - \frac{1}{(X^2-1)} + \frac{Cr^2}{2(1+Cr^2)^2} \left[\frac{5}{4(1-X^2)} - \frac{2a_1(1-X^2)}{X^2(a_1+a_2X)} + K - \frac{7}{4} \right]}{\frac{(K-1)(3+Cr^2)}{(1+Cr^2)^2} - \frac{Cr^2}{2(1+Cr^2)^2} \left[\frac{5}{4(1-X^2)} - \frac{2a_1(1-X^2)}{X^2(a_1+a_2X)} + K - \frac{7}{4} \right]} \quad (44)$$

In Fig. (11), the factor ω has been plotted against the fractional radial coordinate (r/R). We can see in this figure that, throughout the interior of stars, the ratio $\omega = p/\rho$ is less than unity. This result implies that, inside the stars, densities are dominating over the corresponding pressures everywhere and therefore the underlying fluid distribution is non-exotic in its nature [41].

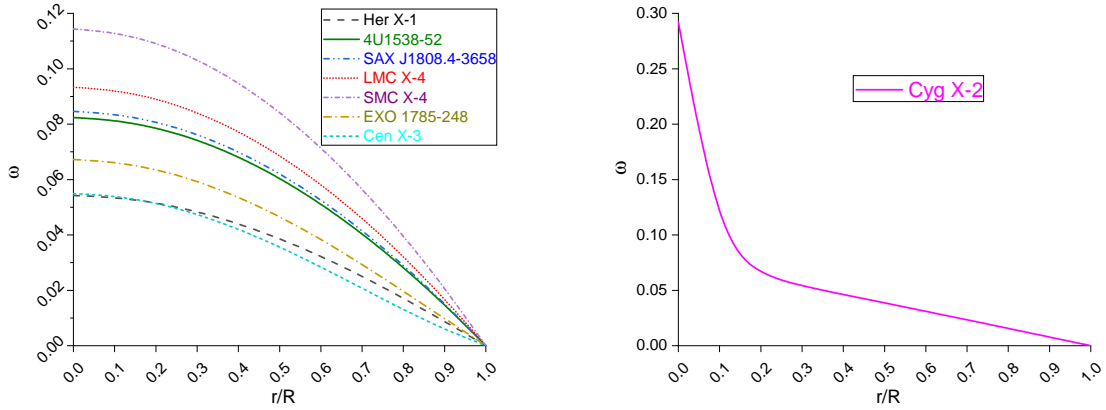


Fig. 11 Ratio of pressure to that of density with respect to fractional radius (r/R) for star candidates Her X-1, 4U 1538-52, SAX J1808.4-3658, LMC X-4, SMC X-4, EXO 1785-248, Cen X-3 ($K < 0$) and Cyg X-2 ($K > 1$).

4.9 Energy Conditions

It is justifiable to expect this model to satisfy the energy conditions within the framework of general relativity. There exists a linear relationship between energy density and pressure, obeying certain restrictions. This is termed as energy conditions. To enhance our investigation on the structure of relativistic space-time, let's examine the following conditions [43]:

1. Dominant energy condition (DEC): $\rho - p \geq 0$
2. Null energy condition (NEC): $\rho + \frac{q^2}{8\pi r^4} \geq 0$
3. Weak energy condition (WEC): $\rho - p + \frac{q^2}{4\pi r^4} \geq 0$
4. Strong energy condition (SEC): $\rho - 3p + \frac{q^2}{4\pi r^4} \geq 0$

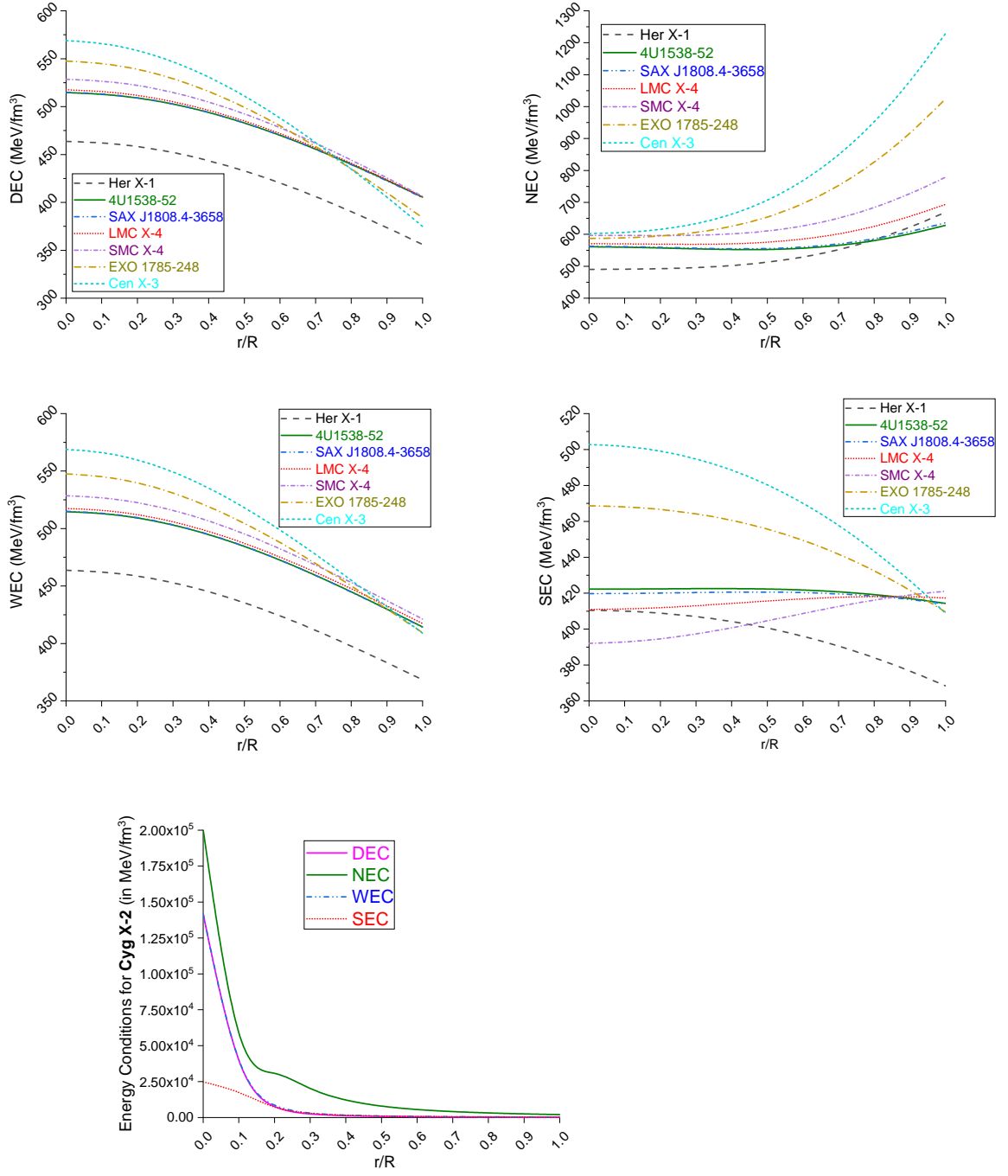


Fig. 12 Energy conditions on the system with respect to fractional radius (r/R) for star candidates Her X-1, 4U 1538-52, SAX J1808.4-3658, LMC X-4, SMC X-4, EXO 1785-248, Cen X-3 ($K < 0$) and Cyg X-2 ($K > 1$).

Nature of energy conditions for considered star candidates has been shown in Fig. (12). We can see that all the energy conditions are satisfied throughout the interior region of the spherical distribution.

4.10 Generalized Tolman-Oppenheimer-Volkov Equation

A star remains in hydrostatic equilibrium under different forces, namely, gravitational force (F_g), hydrostatic force (F_h) and electric force (F_e). Let's consider the generalized Tolman-Oppenheimer-Volkoff equation in the presence of charge [44]

$$\frac{-M_G(\rho + p)}{r^2} e^{(\lambda - \nu)/2} - \frac{dp}{dr} + \sigma \frac{q}{r^2} e^{\lambda/2} = 0, \quad (45)$$

where $M_G(r)$ is the effective gravitational mass of the star within radius r and is defined by

$$M_G(r) = \frac{1}{2} r^2 \nu' e^{(\nu - \lambda)/2} \quad (46)$$

Substituting the value of $M_G(r)$ in eq. (45), we obtain,

$$F_g + F_h + F_e = 0 \quad (47)$$

where,

$$\begin{aligned} F_g &= -\frac{\nu'}{2}(\rho + p) = -\frac{C^2 r}{16\pi} \left[\frac{P_1 P_2 + P_3 P_4}{P_2 P_5} \right] \left[\frac{2}{K(K-1)(X^2-1)^2} + \frac{X^2}{K(X^2-1)} \frac{P_1 P_2 + P_3 P_4}{P_2 P_5} \right], \\ F_h &= -\frac{dp}{dr} = -\frac{C^2 r}{8\pi} \left[\frac{X^2}{K(X^2-1)^2} \frac{D}{P_2 P_5} + \frac{2}{K(1-K)(X^2-1)^2} \left(\frac{P_1 P_2 + P_3 P_4}{P_2 P_5} - 1 \right) + D_7 + D_8 \right], \\ F_e &= \sigma \frac{q}{r^2} e^{\lambda/2} = \frac{1}{8\pi r^4} \frac{dq^2}{dr} = \frac{C^2 r}{8\pi} \left[\frac{3 + Cr^2}{K(1 + Cr^2)^3} \left\{ \frac{5}{4(1-X^2)} - \frac{2a_1(1-X^2)}{X^2(a_1 + a_2 X)} + K - \frac{7}{4} \right\} + D_8 \right]. \end{aligned}$$

We have drawn figures for each compact star candidates to show the behaviour of these forces. It is evident from fig (13) that F_g nullifies the combined effect of F_h and F_e . In other words, the static equilibrium is attainable under these three different forces for this model.

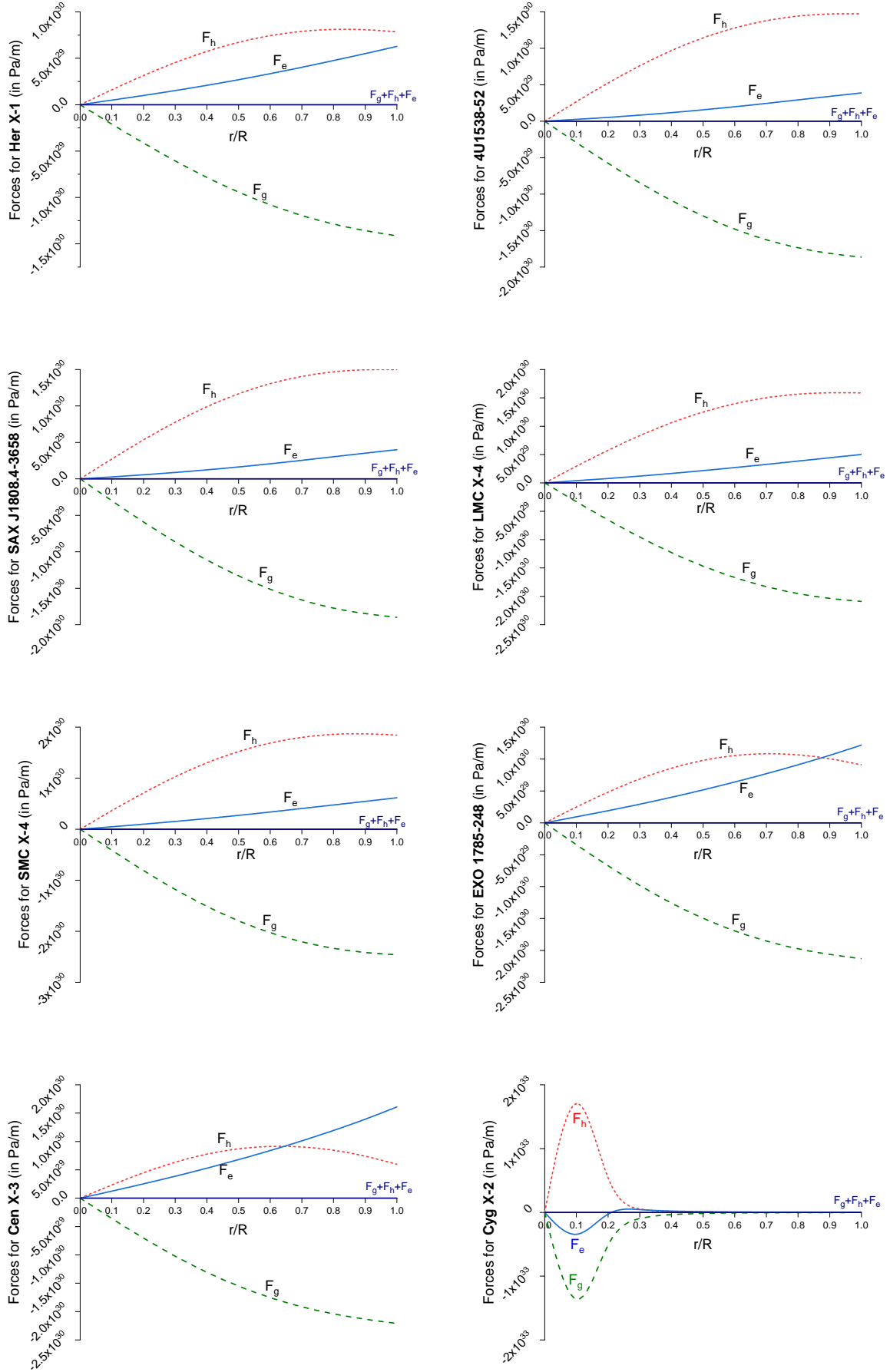


Fig. 13 Variations of gravitational force (F_g), hydrostatic force (F_h) and electric force (F_e) acting on the system with respect to fractional radius (r/R) for star candidates Her X-1, 4U 1538-52, SAX J1808.4-3658, LMC X-4, SMC X-4, EXO 1785-248, Cen X-3 ($K < 0$) and Cyg X-2 ($K > 1$).

4.11 Relativistic Adiabatic Index

The adiabatic index

$$\gamma = \left(\frac{c^2 \rho + p}{p} \right) \left(\frac{dp}{c^2 d\rho} \right) \quad (48)$$

is related to the stability of a stellar configuration. For an isotropic star to be in stable equilibrium, γ must have values strictly greater than $\frac{4}{3}$ throughout the region.

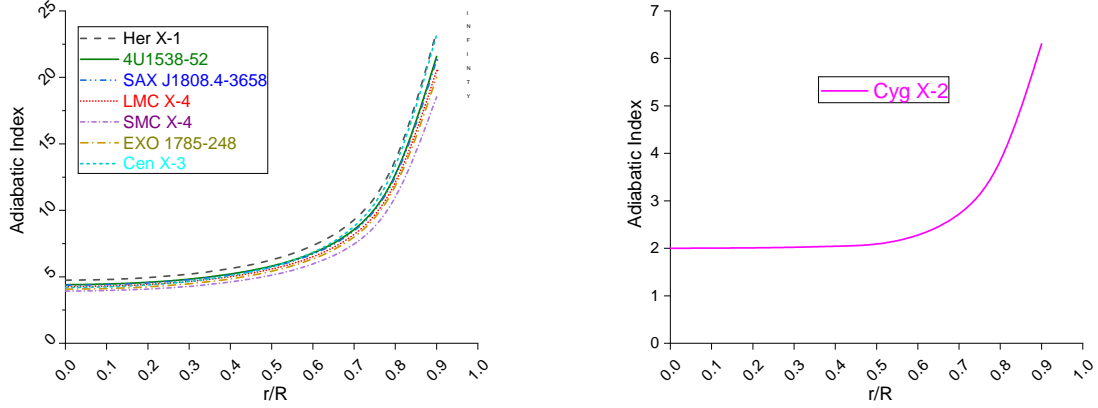


Fig. 14 Variation of adiabatic index with respect to fractional radius (r/R) for star candidates Her X-1, 4U 1538-52, SAX J1808.4-3658, LMC X-4, SMC X-4, EXO 1785-248, Cen X-3 ($K < 0$) and Cyg X-2 ($K > 1$).

Graphs in fig. (14) represent the behavior of adiabatic index γ . We can see that the desirable features have been obtained for each star candidate that we have considered.

4.12 Harrison-Zeldovich-Novikov Stability Criterion

Harrison-Zeldovich-Novikov criterion [46, 47] states the condition for stability of a compact object. According to this criterion, to have a stable configuration, mass of a compact star should increase with increase in central density throughout the stellar region. Mathematically, $\frac{dM}{d\rho_0} > 0$

We can obtain the expression for central density from eq. (28) as

$$\rho_0 = \frac{3C(K-1)}{8\pi K} \quad (49)$$

Let's write M in terms of ρ_0 using eqs. (32) and (49) as

$$M = 4\pi R^3 \frac{\rho_0}{M_1} \left[K - 1 + 4\pi K R^2 \rho_0 \frac{M_2}{M_1} \right] \quad (50)$$

where,

$$M_1 = 3(K-1) + 8\pi K \rho_0 R^2,$$

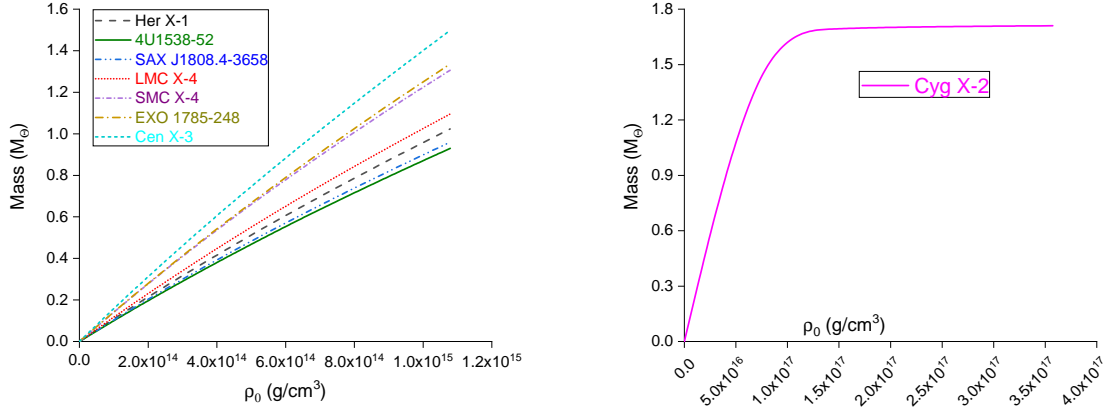


Fig. 15 Variation of mass function with respect to density for star candidates Her X-1, 4U 1538-52, SAX J1808.4-3658, LMC X-4, SMC X-4, EXO 1785-248, Cen X-3 ($K < 0$) and Cyg X-2 ($K > 1$).

$$M_2 = \left[-\frac{15}{4} \frac{(1-K)^2}{M_1} - \frac{2a_1 M_1}{3(1-K)^2 X_1^2 (a_1 + a_2 X_1)} + K - \frac{7}{4} \right].$$

We can observe in fig (15) that mass of every star is positive definite and it increases with increase in central density. Thus, we can conclude that the presented model satisfies Harrison-Zeldovich-Novikov criterion of stability.

5 Conclusion

In this paper, we have investigated the nature of isotropic compact stars. By employing the Vaidya and Tikekar ansatz for metric potential, we have simplified the Einstein field equations and obtained exact solutions for isotropic compact stars. Based on physical requirements, we equated the interior solution to the exterior one (Reissner-Nördstro solution) at surface to fix the value of constants A_1 and A_2 . Using these values of constants and free parameters C and K it is possible to determine mass and radius for compact stars. To refine the model further, we have shown through graphs, that metric potentials are regular, energy density and pressure are finite at the center and monotonically decreasing towards the boundary. The pressure vanishes at the boundary. The electric field intensity is zero at centre and it increases towards the surface. We have shown that the model is compatible with the compact objects such as, Her X-1, 4U 1538-52, SAX J1808.4-3658, LMC X-4, SMC X-4, EXO 1785-248, Cen X-3 and Cyg X-2. As shown in Table 2, the gravitational redshift is bounded above function and satisfies $z_s < 2$. Adiabatic index is strictly greater than $\frac{4}{3}$ throughout the model. The model satisfies the TOV equation, energy conditions, the causality condition and it also fullfills Harrison-Zeldovich-Novikov criterion. This shows that the obtained model is stable. To obtain numerical values of physical quantities, we have taken $G = 6.674 \times 10^{-11} \text{N/ms}^2$, $c = 3 \times 10^8 \text{m/s}$, $1M_\odot = 1.475 \text{km}$ and have multiplied charge by 1.1659×10^{20} to convert it from relativistic unit (km) to coulomb.

As a future scope, we can look for other forms of metric potentials which could possess more general behaviour and thus it might be able to describe other types of compact objects.

Acknowledgments

The Authors are sincerely grateful towards Science and Engineering Research Board (SERB), DST, New Delhi for providing the needed financial support. They are also very humbled towards the Department of Mathematics, Central University of Jharkhand, Ranchi, India, where the paper has been written and finalized, for the much needed support.

Appendix A: Notations used in eqs (29), (30) and (31)

$$\begin{aligned}
 P_1 &= \frac{2}{(K-1)X} \left(\frac{a_1+a_2X}{2(X^2-1)} - \frac{a_1}{X^2} \right), \quad P_2 = \frac{a_1}{a_2^2} S(X) + \frac{A_2}{A_1}, \quad P_3 = \frac{a_1}{a_2^2(K-1)X^2}, \quad P_4 = \sec^2 \left(\tan^{-1} \sqrt{\frac{a_2X}{a_1}} \right) + \\
 &\cos^2 \left(\tan^{-1} \sqrt{\frac{a_2X}{a_1}} \right) - 2, \quad P_5 = \left(\frac{a_1+a_2X}{X} \right) \\
 D(r) &= D_1P_2 + D_2P_1 + D_3P_4 + D_4P_3 - \left(\frac{P_1P_2+P_3P_4}{P_2P_5} \right) (D_2P_5 + D_5P_2), \\
 D_1(r) &= -\frac{P_1}{(K-1)X^2} + \frac{2}{(K-1)^2X^2} \left[\frac{a_2}{2(X^2-1)} - \frac{X(a_1+a_2X)}{(X^2-1)^2} + \frac{2a_1}{X^3} \right], \quad D_2(r) = \frac{a_1}{2a_2^2(K-1)} \frac{P_4}{X(a_1+a_2X)}, \quad D_3(r) = \\
 &\frac{-2a_1}{(K-1)^2a_2^2X^4}, \quad D_4(r) = \frac{a_2}{(K-1)X(a_1+a_2X)} \left\{ \sec^2 \left(\tan^{-1} \sqrt{\frac{a_2X}{a_1}} \right) - \cos^2 \left(\tan^{-1} \sqrt{\frac{a_2X}{a_1}} \right) \right\}, \quad D_5(r) = \\
 &\frac{-a_1}{(K-1)X^3}, \quad D_6(r) = \frac{2(1-K)(5+Cr^2)}{K(1+Cr^2)^3}, \quad D_7(r) = \frac{1-Cr^2}{K(1+Cr^2)^3} \left[\frac{5}{4(1-X^2)} - \frac{2a_1(1-X^2)}{X^2(a_1+a_2X)} + K - \frac{7}{4} \right], \quad D_8(r) = \\
 &\frac{Cr^2}{4K(K-1)(1+Cr^2)^2} \left[\frac{-5}{(1-X^2)^2} + \frac{8a_1}{X^2(a_1+a_2X)} + \frac{4a_1(1-X^2)(2a_1+3a_2X)}{X^4(a_1+a_2X)^2} \right].
 \end{aligned}$$

Appendix B : Finding constants A_1 & A_2

Here we are going to calculate the values of arbitrary constants A_1 and A_2 , used in eq. (26), using boundary conditions (32,33).

First we are going to determine the value of $\frac{A_2}{A_1}$. Using boundary condition $p(R) = 0$ in eq. (29), we can obtain the following relationship

$$-\frac{P_{31}P_{41}(K+CR^2)}{P_{11}(K+CR^2) + (1-K)(J_1+1)P_{51}} = P_{21} = \frac{a_1}{a_2^2} S(X_1) + \frac{A_2}{A_1} \quad (51)$$

Thus, we have

$$\frac{A_2}{A_1} = \left[\frac{P_{31}P_{41}X_1^2}{(J_1+1)P_{51} - P_{11}X_1^2} - \frac{a_1}{a_2^2} S(X_1) \right] \quad (52)$$

where,

$$\begin{aligned}
 X_1 &= \sqrt{\frac{K+CR^2}{K-1}}, \quad J_1 = \frac{CR^2(1-X_1^2)}{2(1+CR^2)^2} \left[\frac{5}{4(1-X_1)} - \frac{2a_1(1-X_1^2)}{X_1^2(a_1+a_2X_1)} + K - \frac{7}{4} \right], \quad P_{11} = \frac{2}{(K-1)X_1} \left(\frac{a_1+a_2X_1}{2(X_1^2-1)} - \right. \\
 &\left. \frac{a_1}{X_1^2} \right), \quad P_{31} = \frac{a_1}{a_2^2(K-1)X_1^2}, \quad P_{41} = \sec^2 \left(\tan^{-1} \sqrt{\frac{a_2X_1}{a_1}} \right) + \cos^2 \left(\tan^{-1} \sqrt{\frac{a_2X_1}{a_1}} \right) - 2, \quad \& \quad P_{51} = \\
 &\left(\frac{a_1+a_2X_1}{X_1} \right).
 \end{aligned}$$

To find the value of A_1 , we will use the condition $Z^2(R) = \frac{K+CR^2}{K(1+CR^2)}$. After a little bit of computation, we can obtain the values of A_1 and A_2 as,

$$\begin{aligned}
 A_1 &= \frac{1}{\sqrt{K}(1-X_1^2)^{3/4}} \left[\frac{(J_1+1)P_{51} - P_{11}X_1^2}{(a+bX_1)P_{31}P_{41}} \right], \quad \text{when } K < 0 \\
 A_1 &= \frac{1}{\sqrt{K}(X_1^2-1)^{3/4}} \left[\frac{(J_1+1)P_{51} - P_{11}X_1^2}{(a+bX_1)P_{31}P_{41}} \right], \quad \text{when } K > 1
 \end{aligned} \quad (53)$$

and

$$A_2 = \frac{1}{\sqrt{K}(1 - X_1^2)^{3/4}} \left[\frac{X_1^2}{a_1 + a_2 X_1} - \frac{a_1 (J_1 + 1)(P_{51} - P_{11} X_1^2)}{a_2^3 (a_1 + a_2 X_1) P_{31} P_{41}} S(X_1) \right], \text{ when } K < 0$$

$$A_2 = \frac{1}{\sqrt{K}(X_1^2 - 1)^{3/4}} \left[\frac{X_1^2}{a_1 + a_2 X_1} - \frac{a_1 (J_1 + 1)(P_{51} - P_{11} X_1^2)}{a_2^3 (a_1 + a_2 X_1) P_{31} P_{41}} S(X_1) \right], \text{ when } K > 1. \quad (54)$$

Appendix C: Structural properties of compact stars in relativistic units

Table 4 Structural properties of “Her X-1” within radius.

r/R	$q(km)$	$\rho(km^{-2})$	$\sigma(km^{-2})$	$p(km^{-2})$	p/ρ	v_s^2	γ
0	0	0.000647295	0.000343118	3.51166×10^{-5}	0.054246	0.243597	4.73422
0.2	0.0062208	0.000638455	0.000341655	3.29828×10^{-5}	0.051653	0.241651	4.919966
0.4	0.0519939	0.000612955	0.000337174	2.70386×10^{-5}	0.044117	0.235845	5.58173
0.6	0.1854576	0.000573693	0.000329066	1.85338×10^{-5}	0.032308	0.226207	7.227869
0.8	0.4631823	0.0005246	0.000316964	9.02301×10^{-6}	0.017206	0.212543	12.565491
0.1	0.9437229	0.000469944	0.000301478	0	0	0.194044	<i>Inf</i>

Table 5 Structural properties of “4U 1538-52” within radius.

r/R	$q(km)$	$\rho(km^{-2})$	$\sigma(km^{-2})$	$p(km^{-2})$	p/ρ	v_s^2	γ
0	0	0.000740376	0.000250639	6.09788×10^{-5}	0.082368	0.335101	4.403433
0.2	0.004255506	0.000730016	0.000249992	5.75363×10^{-5}	0.078808	0.333976	4.571807
0.4	0.037426428	0.000700214	0.000248053	4.7823×10^{-5}	0.068302	0.330724	5.172831
0.6	0.140156388	0.000654508	0.000243333	3.35844×10^{-5}	0.051301	0.325676	6.673971
0.8	0.362087712	0.00059778	0.000233507	1.69538×10^{-5}	0.028372	0.319259	11.572042
0.1	0.750605184	0.000535233	0.000217701	0	0	0.311849	<i>Inf</i>

Table 6 Structural properties of “SAX J1808.4-3658” within radius.

r/R	$q(km)$	$\rho(km^{-2})$	$\sigma(km^{-2})$	$p(km^{-2})$	p/ρ	v_s^2	γ
0	0	0.000742648	0.000256223	6.28298×10^{-5}	0.084607	0.339965	4.358118
0.2	0.004484364	0.000732097	0.000255369	5.92707×10^{-5}	0.080957	0.338846	4.52437
0.4	0.039317695	0.000701789	0.000252743	4.92578×10^{-5}	0.070181	0.335617	5.117791
0.6	0.146719803	0.000655363	0.000247017	3.45627×10^{-5}	0.052735	0.330607	6.599795
0.8	0.377966687	0.000597816	0.000236071	1.74475×10^{-5}	0.029183	0.324236	11.434827
0.1	0.781734369	0.00053448	0.000219208	0	0	0.316856	<i>Inf</i>

Table 7 Structural properties of “LMC X-4” within radius.

r/R	$q(km)$	$\rho(km^{-2})$	$\sigma(km^{-2})$	$p(km^{-2})$	p/ρ	v_s^2	γ
0	0	0.000753411	0.000299159	7.02981×10^{-5}	0.093311	0.362564	4.248113
0.2	0.00589371	0.000742309	0.000296924	6.63071×10^{-5}	0.089316	0.361449	4.40832
0.4	0.05038707	0.000710469	0.000290393	5.506×10^{-5}	0.077505	0.358201	4.979845
0.6	0.183568314	0.000661794	0.000279131	3.8603×10^{-5}	0.05833	0.353044	6.405616
0.8	0.464499057	0.000601669	0.000262529	1.94611×10^{-5}	0.032339	0.34615	11.049986
0.1	0.950041149	0.000535754	0.000241138	0	0	0.337298	<i>Inf</i>

Table 8 Structural properties of “SMC X-4” within radius.

r/R	$q(km)$	$\rho(km^{-2})$	$\sigma(km^{-2})$	$p(km^{-2})$	p/ρ	v_s^2	γ
0	0	0.00078779	0.000325954	9.00668×10^{-5}	0.114335	0.402212	3.920058
0.2	0.007727125	0.000774608	0.000322645	8.47967×10^{-5}	0.109471	0.401061	4.064701
0.4	0.065923415	0.00073696	0.00031308	7.00762×10^{-5}	0.095082	0.397692	4.580329
0.6	0.239090494	0.000680079	0.000297205	4.8752×10^{-5}	0.071677	0.392261	5.864862
0.8	0.601355776	0.000610913	0.00027515	2.43375×10^{-5}	0.039836	0.384667	10.040912
0.1	1.222634288	0.000536426	0.000248761	0	0	0.373824	<i>Inf</i>

Table 9 Structural properties of “EXO 1785-248 ” within radius.

r/R	$q(km)$	$\rho(km^{-2})$	$\sigma(km^{-2})$	$p(km^{-2})$	p/ρ	v_s^2	γ
0	0	0.000774921	0.000455298	5.20913×10^{-5}	0.067224	0.256364	4.069953
0.2	0.010760384	0.00076072	0.00045185	4.849×10^{-5}	0.063746	0.253618	4.232158
0.4	0.089843897	0.000720288	0.000441454	3.87205×10^{-5}	0.053752	0.245302	4.808875
0.6	0.319227675	0.000659461	0.000424342	2.53624×10^{-5}	0.03846	0.230946	6.2358
0.8	0.792950041	0.00058589	0.000401993	1.15446×10^{-5}	0.019701	0.208868	10.810668
0.1	1.609960513	0.000506878	0.000378189	0	0	0.174329	<i>Inf</i>

Table 10 Structural properties of “Cen X-3 ” within radius.

r/R	$q(km)$	$\rho(km^{-2})$	$\sigma(km^{-2})$	$p(km^{-2})$	p/ρ	v_s^2	γ
0	0	0.000794746	0.000514889	4.36632×10^{-5}	0.054945	0.218321	4.191785
0.2	0.013555906	0.000778471	0.000510378	4.0173×10^{-5}	0.051602	0.214795	4.377354
0.4	0.11279762	0.000732397	0.000496939	3.09014×10^{-5}	0.042185	0.204072	5.041574
0.6	0.398940126	0.00066378	0.000475404	1.88637×10^{-5}	0.028424	0.185362	6.706768
0.8	0.98686445	0.000581808	0.000448432	7.57399×10^{-6}	0.013016	0.156026	12.14358
0.1	2.000262498	0.00049485	0.000421627	0	0	0.108787	<i>Inf</i>

Table 11 Structural properties of “Cyg X-2 ” within radius.

r/R	$q(km)$	$\rho(km^{-2})$	$\sigma(km^{-2})$	$p(km^{-2})$	p/ρ	v_s^2	γ
0	0	0.264256351	0.246886517	0.07718148	0.292071	0.513242	2.000395
0.2	0.37743189	0.007328578	0.001769387	0.000466881	0.063707	0.158856	2.008239
0.4	0.91447395	0.001657421	0.000655655	7.66333×10^{-5}	0.046239	0.090316	2.04356
0.6	1.417686	0.000719241	0.000307866	2.23442×10^{-5}	0.031063	0.067565	2.242633
0.8	1.91133324	0.000401051	0.000176378	6.28475×10^{-6}	0.015668	0.054466	3.530793
1.0	2.40103323	0.000255633	0.000113835	0	0	0.044416	<i>Inf.</i>

References

1. K. Schwarzschild: Sitzber. Preuss. Akad. Wiss. Berlin **189**, 424 (1916). Republished in Gen. Relativ. Gravit. **35**, 951 (2003)
2. M. S. R. Delgaty, K. Lake: Comput. Phys. Commun. **115**, 395 (1998)
3. H. Stephani, D. Kramer, M. MacCallum, C. Hoenselaers and E. Herlt: Exact Solutions of the Einstein Field Equations (Cambridge University Press, Cambridge, 2003)
4. A. DeBenedictis, R. Garattini, F.S.N. Lobo: Phys. Rev. D **78**, 104003 (2008)
5. F. Rahaman, A.K. Yadav, S. Ray, R. Maulick, R. Sharma: Gen. Relativ. Grav. **44**, 107 (2011)
6. R. C. Tolman: Phys. Rev. **55**, 364 (1939)
7. M. Wyman: Phys. Rev. **75**, 1930 (1949)
8. G. K. Patwardhan, P. C. Vaidya: J. Univ. Bombay **12**, 23 (1943). Part III
9. H. A. Buchdahl: Phys. Rev. **116**, 1027 (1959)
10. B. Kuchowicz: Phys. Lett. A **25**, 419 (1967b)
11. B. Kuchowicz: Acta Phys. Pol. **33**, 541 (1968a)
12. B. Kuchowicz: Acta Phys. Pol. **34**, 131 (1968b)
13. S. Bayin : Phys. Rev. D **18**, 2745 (1978)
14. P. C. Vaidya, R. Tikekar: J. Astrophys. Astron. **3**, 325 (1982)
15. M. R. Finch, J. E. F. Skea: Class. Quantum Gravity **6**, 467 (1989)
16. S. Mukherjee, B. C. Paul, N. K. Dadhich: Class. Quantum Gravity **14**, 3475 (1997)
17. Y. K. Gupta, M. K. Jasim: Astrophys. Space Sci. **272**, 403 (2000)
18. K. Komathiraj, S.D. Maharaj: J. Math. Phys. **48**, 042501 (2007)
19. N. Bijalwan, Y.K. Gupta: Astrophys. Sp. Sci. **334**, 223 (2011)
20. N. Bijalwan, Y.K. Gupta: Astrophys. Sp. Sci. **337**, 455462 (2012)
21. L. K. Patel, Kopper: Aust. J. Phys. **40**, 441 (1987)
22. R. Sharma, S. Mukherjee, S. D. Maharaj: Gen. Relat. Gravity **33**, 999 (2001)
23. Y.K. Gupta, M. Kumar: Gen. Relat. Gravity **37**, 575 (2005)
24. Y. K. Gupta, M. Kumar: Astrophysics and Space Science. **299**, 43 (2005)
25. K. Komathiraj, S. D. Maharaj: Int. J. Mod. Phys. D **16**, 1803 (2007)
26. J. Kumar, Y. K. Gupta: Astrophys Space Sci. **345**, 331 (2013).
27. J. Kumar, Y. K. Gupta: Astrophys Space Sci. **351**, 243 (2014)
28. L. D. Landau, E. M. Lifshitz: Pergamon Press, Oxford, England. 225 (1975)
29. M. P. Korkina and O. Y. Orlyanskii: Ukr. Fiz. Zh. **36**, 127 (1991) [Ukr. J. Phys. **36**, 885 (1991)]
30. J. Kumar, A. K. Prasad, S. K. Maurya, A. Banerjee: Eur. Phys. J. C. **78** (7), 1 (2018)
31. J. Kumar, P. Bharti (2021) arXiv:2102.13489.
32. A. K. Prasad, J. Kumar, S. K. Maurya, B. Dayanandan: Astrophysics and Space Science. **364**, 66 (2019)
33. J. Kumar, S. K. Maurya, A. K. Prasad, A. Banerjee, Journal of Cosmology and Astroparticle Physics, **11**, 005 (2019)
34. A. K. Prasad, J. Kumar, A. Kumar, Arabian Journal of Mathematics, **10**, 669 (2021)
35. A. K. Prasad, J. Kumar: Astrophysics and Space Science **366** (3), 1 (2021)
36. J. Kumar, P. Bharti, Phys. Rev. D **104**, 083009 (2021)
37. P. S. Florides, J. Phys. A Math. Gen. **17**, 1419 (1983)
38. H. Bondi: Proc. R. Soc. A **282**, 303 (1964)
39. C.G. Böhmer, T. Harko, Gen. Relat. Gravit. **39**, 757 (2007)
40. H. Andreasson, J. Phys. Conf. Ser. **189**, 012001 (2009)
41. F. Rahaman, S.A.K. Jafry, K. Chakraborty, Phys. Rev. D **82**, 104055 (2010)

- 42. N. Straumann: General Relativity and Relativistic Astrophysics (Springer, Berlin, 1984), p. 43.
- 43. S. K. Maurya, Y. K. Gupta, S. Ray, V. Chatterjee: *Astrophys Space Sci* **361**, 351 (2016)
- 44. J. P. de Leon: *Gen. Rel. Grav.* **25**, 1123 (1993)
- 45. V. Canuto: in *Solvay Conference on Astrophysics and Gravitation*, Brussels, 1973 ISBN 10: 2800405961.
- 46. B. K. Harrison et al.: *Gravitational Theory and Gravitational Collapse*. University of Chicago Press, Chicago (1965)
- 47. Ya. B. Zeldovich, I. D. Novikov: *Relativistic Astrophysics Vol.1: Stars and Relativity*. University of Chicago Press, Chicago (1971)
- 48. K. Lake: *Phys. Rev. D.* **67**, 104015 (2003)
- 49. S. Ray, A. L. Espindola, M. Malheiro, J. P. S. Lemos, V. T. Zanchin: *Phys. Rev. D.* **68**, 084004 (2003)